

Vertical Transport and Mixing in Complex Terrain Airsheds: Implementation of a Stable PBL Turbulence Parameterization for the Mesoscale Model MM5

1. Introduction

In contrast to its daytime unstable counterpart, the progress in understanding and parameterizing turbulence in nocturnal stable boundary layer has been slow due to complexities associated with turbulence in stably stratified flows (Mahrt et al., 1999; Riley and Lelong, 2000). Stable stratification readily induces drainage flows over uneven topography (Whiteman, 2000), causes intermittent turbulence (Nieuwstadt, 1984) and lead to intriguing phenomena such as highly sheared low-level jets, linear and non-linear gravity waves, flow blocking, intusions and meandering (Bluemen, 1990; Fernando 2002), thus posing great challenges to the quantification of the effects of stable stratification in numerical models (Louis, 1979; Brown et al., 1994; McNider et al., 1995; Derbyshire, 1999). Numerous efforts have been made toward understanding turbulence in the atmospheric boundary layer, especially through recent field campaigns such as the Vertical Transport and Mixing (VTMX) (Doran et al., 2002), CASES (Poulos et al., 2002) and Rotach et al. (2004) research initiatives, yet incorporation of new knowledge in predictive models has occurred slowly and nocturnal flow simulations continue to be plagued with unacceptable levels of uncertainties. Concluding an evaluation of three state-of-the-art mesoscale numerical models (MM5, RAMS and Meso-eta) conducted at horizontal resolutions finer than 1km, Zhong and Fast (2003) pointed out major

difficulties associates with predictions, which included biases toward weaker nocturnal inversion strengths and colder near-surface temperatures. They attributed such difficulties to the four default turbulent parameterization schemes of MM5 that they used in their simulations. Zhang and Zheng (2004) compared five turbulent parameterization schemes and found that the predictions are notably sensitive to the type of parameterization used. All of these studies emphasized the importance of developing better radiation and turbulent mixing parameterizations to improve predictions. Such improvements are particularly necessary, given that demand for accurate mesoscale-model predictions is ever increasing due to increased emphasis of air quality predictions and regulations, growing engineering applications of meteorology such as power demand calculations as well as urban security needs, such as, emergency response during an accident or a biological/chemical attack.

The simplest turbulent transport parameterization used in air quality and numerical weather prediction models is the first-order closure, the so-called K-theory (e.g. Corrsin, 1974; Wyngaard and Brost, 1984; Holtslag and Moeng, 1991; Stull, 1993). Notwithstanding its simplicity and sound phenomenological basis, the K-theory suffers from striking deficiencies, as a result of which alternative approaches have been developed. Some examples are the modified first-order closure (Townsend, 1980; Troen and Mahrt, 1986; Hong and Pan, 1996), higher-order closure (Mellor and Yamada, 1974; Yamada, 1983; Yamada and Bunker, 1988; Benoit et al., 1989; Janjic, 1990; Ballard et al., 1991; Janjic, 1994; Pan et al., 1994) and non-local exchange schemes (Townsend, 1980; Estoque, 1968; Berkowicz and Prahm, 1979; 1980; Blackadar, 1979; Zhang and

Anthes, 1982; Fiedler, 1984; Troen and Mahrt, 1986; Stull, 1988; 1993; Hong and Pan, 1996).

In spite of its drawbacks, the first order closure based on similarity theory remains the most popular parameterization for stable periods in numerical weather prediction models, although alternative approaches have been used for the daytime convective period [e.g. Blackadar non-local mixing scheme (Zhang and Anthes, 1982); non-local K-theory (Hong and Pan, 1996)]. The diffusivities for stable periods in first order models are formulated using stability dependent profile functions that are built upon basic relations between wind shear, stress and height for neutral conditions. These neutral relations, however, are ambiguous above the surface layer (Derbyshire, 1999).

In an attempt to develop improved turbulent parameterizations for nocturnal periods of mesoscale models, our research group has proposed new semi-empirical eddy diffusivities for heat and momentum based on VTMX data (Monti et al., 2002). This report concerns the implementation of these parameterizations in the Penn State/NCAR Mesoscale Model (MM5), which is one of the most commonly used mesoscale meteorological model in flow and air quality studies. The simulation results are evaluated against field measurements taken during the VTMX campaign (Doran et al., 2002).

In Section 2, brief descriptions of the new and MM5 default parameterization schemes are given. Section 3 describes the configuration of numerical experiments and designs days for simulations. Results of simulation results and pertinent discussions are described in Section 4 and 5, and conclusions of the study are given in Section 6.

2. PBL Parameterization in a Mesoscale Model

2.1. Eddy diffusivities in MM5

MM5 provides multiple options for turbulence parameterizations, thus enabling modification of the model to cater user's specific needs. Its default schemes include the 1st order local K-theory, 1.5 order local closure, non-local turbulence closure, and modified local closure with non-local effects. Interestingly, these various turbulence schemes employ the 1st order local K-theory for the stable condition, while higher order or advanced closure methods are applied for the unstable case.

In our studies of nocturnal planetary boundary layer (PBL), a non-local K-theory known as the MRF (Medium Range Forecast) scheme was employed (Hong and Pan, 1996), considering its (i) simplicity, wide usage and fastness (ii) better or comparable skills to other schemes (Bright and Mullen, 2002; Zhong and Fast, 2003) and (iii) direct coupling with a land-surface scheme of MM5.

The MRF scheme is a modified K-theory, with an additional counter-gradient term that incorporates the contribution of large-scale eddies to the total flux. The turbulence diffusion for the prognostic variable ϕ is expressed as

$$\overline{(w'\phi')} = -K_c \left(\frac{\partial \phi}{\partial z} - \gamma_c \right), \quad (1)$$

where γ_c is the counter-gradient term, w the vertical velocity and z the vertical coordinate.

For mixed-layer diffusion, the counter gradient term is written as

$$\gamma_c = b \frac{\overline{(w'\phi')}_0}{w_s h}, \quad (2)$$

where $\overline{(w'\phi')}_0$ is the surface flux, w_s a mixed-layer velocity scale defined as $w_s = u_* \Phi_m^{-1}$, h the boundary-layer depth, u_* the surface frictional velocity and Φ_m a profile function for momentum; Φ_m is evaluated at the top of the surface layer for computing w_s . The coefficient of proportionality b is set to be 7.8 (Troen and Mahrt, 1986). This non-local flux correction is applied only to temperature and moisture for convective mixing case, but not for stable case. The momentum diffusivity coefficient K_m is formulated as

$$K_m = \kappa w_s z \left(1 - \frac{z}{h}\right)^p, \quad (3)$$

where κ is the von Kármán constant (0.4), z the height from the surface and p a profile shape exponent taken to be 2. The eddy diffusivity for temperature K_h is computed using K_m via the turbulent Prandtl number ($Pr = K_m / K_h$), which is written as

$$Pr = \left(\frac{\Phi_h}{\Phi_m} + b \kappa \frac{h_{SL}}{h} \right), \quad (4)$$

where Φ_h a profile function for heat, b a constant ($=7.8$), h_{SL} , the top of the surface layer, is set to be $0.1h$. For unstable and neutral conditions, Φ_m and Φ_h are defined by

$$\Phi_m = \left(1 - 16 \frac{0.1h}{L}\right)^{-1/4}, \text{ for } u \text{ and } v \text{ components}, \quad (5)$$

$$\Phi_h = \left(1 - 16 \frac{0.1h}{L}\right)^{-1/2}, \text{ for temperature.} \quad (6)$$

For stable conditions, however, the model employs identical profile functions for momentum and heat, viz.

$$\Phi_m = \Phi_h = \left(1 + 5 \frac{0.1h}{L}\right). \quad (7)$$

leading to a constant Prandtl number as defined by (4). Regardless of the prevailing thermal and aerodynamic conditions, therefore, the Prandtl number takes for the value of 1.3 ($K_h = 0.77 K_m$) for stably stratified conditions.

The boundary layer height is calculated as

$$h = Rib_{cr} \frac{\theta_{va} U(h)^2}{g(\theta_v(h) - \theta_s)}, \quad (8)$$

where Rib_{cr} is the critical bulk Richardson number, $U(h)$ the horizontal wind speed at h , θ_{va} the virtual potential temperature at the lowest model level, $\theta_v(h)$ the virtual potential temperature at h , and θ_s the appropriate temperature near the surface defined as

$$\theta_s = \theta_{va} + \theta_T, \quad (9)$$

θ_T is the scaled virtual temperature excess near the surface (Hong and Pan, 1996). The boundary height, h , is obtained iteratively. First, h is estimated by (8) without considering the thermal excess, θ_T . This estimated h is utilized to compute the profile functions in (5) – (7), and to compute the mixed-layer velocity w_s . Using the updated w_s and θ_T , h is enhanced.

2.2. The New Eddy Diffusivity Parameterization

Based on the VTMX data and considering local governing parameters, Monti et al. (2002) suggested a new parameterization for eddy diffusivities for stable atmosphere. They presented two forms of diffusivities, one a dimensional form (following the tradition of ocean general circulation models; see Pacanowski and Philander, 1981; Garget and Holloway, 1992) and the other a dimensionless form consistent with

appropriate local velocity and length scales. The dimensional eddy diffusivities (in $\text{m}^2 \text{s}^{-1}$) were given by

$$K_m = 0.45 \cdot Ri_g^{0.22} \quad \text{for the entire range of } Ri_g \quad (10)$$

$$K_h = 0.07 \cdot Ri_g^{-0.45} \quad \text{for } Ri_g < 1 \text{ and} \quad (11)$$

$$K_h = 0.07 \quad \text{for } Ri_g > 1, \quad (12)$$

where Ri_g is the averaged value of gradient Richardson number defined as

$$Ri_g = \frac{N^2}{\left| \frac{\partial \tilde{V}}{\partial z} \right|^2} = \frac{N^2}{\left(\frac{\partial \bar{U}}{\partial z} \right)^2 + \left(\frac{\partial \bar{V}}{\partial z} \right)^2},$$

based on the averaged value of N^2 and $|d\tilde{V}/dz|$. Here N is the averaged Brünt-Väisälä

frequency ($N^2 = \frac{g}{\theta} \frac{d\bar{\theta}}{dz}$), \tilde{V} the velocity vector with averaged velocities (U , V) in (E-W,

N-S) directions and θ the potential temperature. Normalized parameterizations based on

the variance of vertical velocity (σ_w) and the shear length-scale ($\sigma_w \cdot \left| \frac{d\tilde{V}}{dz} \right|^{-1}$) (Fernando,

2003) were proposed as

$$\frac{K_m}{\sigma_w^2 / |d\tilde{V}/dz|} = 0.34 \cdot Ri_g^{-0.02} \approx 0.34, \quad (13)$$

and

$$\frac{K_h}{\sigma_w^2 / |d\tilde{V}/dz|} = 0.08 \cdot Ri_g^{-0.49} \approx 0.08 \cdot Ri_g^{-0.5}. \quad (14)$$

In order to avoid cumbersome prognostic calculations, the empirical formula of Stull (1988)

$$\frac{\overline{w'^2}}{u_*^2} = 2.5 \left[1 - \left(\frac{z}{h} \right)^{0.6} \right] \quad (15)$$

was employed to diagnostically calculate the vertical wind variance $\sigma_w^2 = \overline{w'^2}$.

The formulae (10) to (14), through empirically based, encapsulate substantial physics and dynamics of stratified flows. They show that both K_m and K_h are stability (Ri_g) dependent, but these dependencies on Ri_g are different and thus the ratio $Pr = K_m/K_h$ is also stability dependent. This contrasts the constant $Pr (=1.3)$ assumption made in conventional schemes such as MRF and Blackadar scheme, as shown in Fig. 1. The data shown in the figure clearly show that, as $Ri_g \rightarrow 0$, the Pr tends to be unity, indicating equal diffusivities for heat and momentum. However, as Ri_g increases, the turbulence in the flow is inhibited by the stable stratification and thus the momentum and heat transfer by turbulent eddies diminishes. Nonetheless, at strong stratifications, the flow can sustain propagating internal waves that can effectively transport momentum, but not heat, and over a certain range the momentum diffusivity in stable flows can even slightly increase with Ri_g . As a result, the Pr continuously decreases with Ri_g in the range accessible in atmospheric flows. One may, therefore, expect the MRF scheme to show anomalous heat diffusion at higher Ri_g , and hence over-prediction of temperature. This spurious heat diffusion is absent in the modified schemes as they account for sustained momentum diffusion by internal waves in highly stable flows while accounting for drastic reduction in eddy-driven vertical heat transport.

3. Numerical Simulations

3.1. Design Days for Simulation

The area chosen for this study is the complex-terrain basin of Salt Lake City, which is characterized by distinct land-lake and mountain-valley contrasts and for which extensive measurements are available through the VTMX field campaign conducted in October 2000 (Doran et al., 2002). Two periods of the VTMX campaign were selected for simulations: 0000 UTC 6 October – 1200 UTC 8 October (IOPs 2 and 3, hereafter, referred to as the Day 7 case) and 1200 UTC 15 October – 0000 UTC 18 October (IOPs 6 and 7; henceforth Day 16 case). The local time lags 7 hours from the UTC time.

As for the synoptic weather condition, the Day 16 case belongs to the ‘well-developed drainage circulation’ category defined by Doran et al. (2002). This period was characterized by clear skies, weak winds aloft the crest level, strong nocturnal radiation inversions, and pronounced drainage flow into the Salt Lake Valley from the surrounding mountains. Conversely, the Day 7 case belongs to the category ‘modulated by synoptic and mesoscale weather system,’ wherein the Salt Lake Valley was influenced by a strong outbreak of cold air to the east of the Continental Divide (Doran et al., 2002). In addition, this case was influenced by a northward propagating thermal low, originated in the southwestern states and northwestern Mexico along the edge of a high pressure located over the middle of the North American continent, thereby causing a noticeable warming trend. The selection of two cases with distinct synoptic weather conditions is intended to provide a robust evaluation of the model performance and hence the efficacy of underlying turbulent parameterizations.

3.2. Numerical Model Configuration

MM5 simulations were conducted with 4 nested domains, having grid resolutions of 54 km, 18 km, 6 km and 2 km. The innermost domain spans 150 km x 120 km in E-W and N-S direction, respectively, which included urban Salt Lake City as well as its surrounding mountains and lakes. The model employed 31 layers vertically, the lowest computational layer being approximately 10 m agl and the top 100 hPa. The NCEP (National Center for Environmental Prediction) *Eta* model output (Grid 212, 40 km grid spacing) together with vertical soundings and surface measurements were used to compile initial and boundary values for the outermost domain as well as for the data assimilation to MM5. MRF PBL scheme, cloud radiation, and simple ice microphysics scheme were chosen for simulations after carefully considering various available options of MM5. Betts-Miller and Kain-Fritsch cumulus schemes were employed for domains 1 and 2, respectively, but no cumulus parameterization was used for the two inner domains considering dry weather conditions encountered. For land surface scheme, we employed five-layer soil model, in which temperature is predicted in 1, 2, 4, 8, and 16 cm deep layers from the surface with fixed substrate below using vertical diffusion equation. Other available options for land surface model such as Noah LSM (Chen and Dudhia, 2001) and Pleim-Xiu LSM (Xiu and Pleim, 2000) were also tested but yielded essentially similar results as the five-layer soil model (not presented). As such, the latter was chosen as the default land surface scheme for the presented study.

The simulation program consisted of ‘Control’ runs with the original MRF scheme and ‘modified’ simulations with two new types of parameterizations (10)–(14). The first modification included implementation of (10), (11) and (12) for the stable ($Ri_g > 0$)

regime; the corresponding simulations are referred to as Modification 1. In the second modification, normalized diffusivities (13) and (14) were implemented for the stable PBL (‘Modification 2’). The simulation results were evaluated using extensive observations made during VTMX field campaign, which consist of meteorological data from surface monitoring stations, sonic anemometers, rawinsondes, and sodars. The measurement sites and topographic features of the modeling domain are shown in Fig. 2.

4. Simulation Results

4.1. Control Runs

In general, control runs successfully generated well-developed thermally driven mountain-valley and land-lake circulations as well as upper atmospheric synoptic conditions. In this paper, however, we focus on model performance in relation to surface temperature and winds, as they are closely linked with eddy diffusivity parameterizations for PBL. Fig. 3 shows time series of surface temperature, wind speed and wind direction taken at VPN10, a special measurement site of VTMX (see Fig. 2), and the predictions of the MRF scheme for the Day 16 case. (The predictions of the modified schemes are also shown, and will be discussed later). Temperature and wind were taken at the height of 1.5 m and 3 m above ground level, respectively. Simulated temperature at the lowest computational layer was interpolated to 2 m temperature according to the surface layer similarity theory, which is a part of the MRF scheme. No such interpolation was made for wind prediction, considering surface wind is typically measured at 10 m agl, the height of the lowest computational layer. Thus, some disparities between predicted and measured are expected due to this height difference. Both the observations and predictions show a

distinct diurnal variation pattern, as observed in previous studies (e.g. Zhang and Zheng, 2004), but the control run predicted colder and warmer temperature, respectively, for daytime and nighttime, than observations.

Considering that the near surface temperature is closely linked to the surface radiational energy budget, we examined the radiation balance at the surface *vis-à-vis* the measurements of incoming solar radiation and outgoing terrestrial radiation measured at the ASU site and the net radiation at the NCAR site. This comparison was intended ensure that no systematic error is embedded in the simulated temperature of the control run. The predicted downward shortwave radiation was in good agreement with the measurements (Fig. 3d). The maximum irradiance of incoming shortwaves on the Day 16 case was about 700 W m^{-2} at 1200 MST, whilst the prediction was 690 W m^{-2} at 1230 MST. The downward component of shortwave flux in MM5 is evaluated by accounting for the effect of solar zenith angle, clouds and clear air with radiation scattering and water vapor absorption.

On the other hand, the reflected component of incoming radiation is modeled by a surface albedo, which is prescribed according to land use and season. With regard to the latter, MM5 assigns summer (April 15 - October 15) and winter (October 15 - April 15) values. For the dominant land use classes in the Salt Lake Valley, i.e. Grassland and Shrubland categories, albedo values of 19 % and 22 %, respectively, are assigned for the summer and 23 % and 25 %, respectively, for the winter. Owing to the somewhat subjective division of seasons, the maximum shortwave insolation for the Day 7 case (750 W m^{-2}) was about 7 % higher than that of Day 16.

In MM5, the outgoing terrestrial radiation is computed using the Stefan-Boltzmann Law, which utilizes the computed ground temperature and an emissivity prescribed according to the land use type. The modeled outgoing longwave radiation, in general, was lower during the convective period and was comparable or somewhat higher during the nocturnal period than the observations. Furthermore, the model consistently over-predicted the net radiation by about 100 W m^{-2} during daytime and about 50 W m^{-2} at night. This over-prediction, together with the daytime cold bias of the model indicates the importance of other terms of the turbulent energy budget in predicting the surface temperature. Since measurements of surface-reflected shortwave and back (longwave) radiation from atmospheric constituents are not available, it is not possible to analyze which radiation component is mainly responsible for this discrepancy. Considering that the incoming shortwave radiation and outgoing nocturnal longwave radiation are in general agreement with the measurements, it is likely that a combination of errors associated with parameterizing back radiation and albedo are responsible for the observed disparity. Conversely, one may argue that it may not be just a modeling issue, but the biases of the measurements that are due to inherent instrumental error, calibration error, artifact of surrounding obstacles, and the representativeness of the monitoring location. Besides, it should be borne in mind that the model predictions and measurements may not represent the same physical quantity. A model produces a volume-averaged quantity. Then, the nearest grid point to the monitoring location is taken for comparisons with the measurements. Also note that a point value can be far from the volume-averaged value depending on the complexity of geometry and the land use category around the monitoring site.

Zhong and Fast (2003) also have commented on the errors associated with the surface energy budget. In their case a significant (45-65%) over-prediction of longwave radiation was noted, which contributed to a nocturnal cold bias. Their simulations differ from ours, in that they did not use data assimilation and also used a different turbulence parameterization (Gayno-Seaman scheme) to be consistent with other models employed in their study. The four-dimensional data assimilation used in the present work can directly alter the forcing-response characteristics through governing equations.

Now we return to our original goal of investigating possible systematic errors associated with the energy budget. If the net radiation, which is consistently over-predicted by the model, is the sole major forcing that sway the near surface temperature, the predicted temperature ought to be warmer than observed. This is not evident from Fig. 3, pointing to the assertion that no major systematic errors on the surface radiation budget have been associated with the temperature prediction of the control run.

The observations show distinct thermally driven circulation patterns (Figs. 3b, c), characterized by northwesterly to westerly up-slope flow during daytime and easterly down-slope flow during nighttime. The daytime winds were stronger and the nocturnal winds were calmer, the former being usually attributed to effective turbulent momentum transfer from the upper atmosphere to the ground level by convective mixing. Although the control run reproduced the temporal variation of the direction of mountain-valley breeze successfully, there were glaring differences between the measured and predicted wind speeds. In particular, the predicted nighttime winds were stronger than observed, alluding to possible overestimation of vertical momentum flux in modeling. Given that the control run employs a constant Prandtl number, this also implies an overestimated

heat flux in the model, which is consistent with the over-prediction of nocturnal temperature in the control run.

4.2. The Modified Schemes

Fig. 3 compares the predictions of control and modified runs. Note that the modifications have been implemented only for stable periods, and hence the three runs produced almost identical daytime temperatures. The nocturnal temperatures of the modified schemes are lower than that of the control run by about 2 K, with the former showing a better fit to the measurements. Modifications 1 and 2 generated quite similar temperatures, although the Modification 2 appears to produce slightly lower temperature than Modification 1.

As will be discussed below, the sensible heat flux shown in Fig. 4a points to a salient mechanism that is responsible for reducing nocturnal temperature in the modified schemes. Although both the models and observations qualitatively exhibit the usual diurnal cycle, the models clearly over-predict the magnitude of the sensible heat flux by more than a factor of 2 for both day and night. The nocturnal flux over-prediction of the control run is also greater so as the corresponding nocturnal temperature compared to the modified runs and measurements (Fig. 3a). Interestingly, although the nocturnal flux is over-predicted, as shown in Fig. 5 the modeled nocturnal inversion strength of the control and (sometimes) the modified runs were smaller than the observed values, at times by a factor of two. For example, averaged temperature lapse rates between 2 m and 55 m level above the ground computed from the control run and Modifications 1 and 2 were 0.047, 0.053 and 0.063 K m⁻¹, respectively, while that from the rawinsonde measurements at the

NCAR site is 0.119 K m^{-1} . Detailed comparison of time series data, however, shows that during late night and in the early morning the inversion strength of the modified runs generally agreed with the measurements, while the control run still under-predicted the inversion strength (Fig. 5). A similar under-prediction has been reported by Zhong and Fast (2003) during their MM5 simulations with Gayno-Seaman scheme.

In terms of the magnitude of eddy diffusion coefficients, modified schemes yielded smaller diffusion coefficients than MRF during the stable period (Fig. 6). Also, note that inverse turbulent Prandtl number from the modified schemes is much smaller than that from the control which is set to a constant 0.7 during nocturnal period.

The above observations can be put into the perspective of the gradient transport equation (1), where $\gamma_c=0$ for nocturnal runs. A high down-gradient flux together with a lower temperature gradient in the PBL for the control runs indicates that the MRF scheme grossly over-predicts the eddy diffusivity for a given stability (Fig. 6a). The larger heat flux toward the surface leads to a higher temperature therein, as observed in Fig. 3a, and to smaller inversion strength as evident from Fig. 5. On the other hand, modified schemes appear to produce more realistic (and reduced) diffusivities, leading to results that are more consistent with the measurements (and their variation with Ri_g without assuming a constant ratio of diffusivities). Note the promising agreement in Fig. 3a between the observed temperature and that predicted by the modified runs.

With respect to the wind speed, the improvements offered by the modified runs were small, if any. Modification 2 decreased wind speed slightly for the nocturnal period, while Modification 1 increased the winds for the same period, and thus the former is a closer fit to the measurement (Fig. 3b). Unlike surface temperature prediction, which is

principally swayed by the radiation balance and surface-atmosphere vertical exchange, the mean near-surface flow is dominated by the pressure gradient forces induced by differential thermal heating (which drives the thermal circulation) as well as synoptic forcing (the influence of which propagates down due to vertical mixing). Owing to these multiple governing factors, the prediction of wind fields and eduction of momentum transfer mechanisms are more challenging and convoluted than its temperature counterpart, which is reflected from the fact that modified parameterizations improve the surface temperature but not the wind fields.

A quantity related to the wind speed is the surface friction velocity u_* , which also determines the vertical *rms* velocity computations in Modification 2 according to (15). The predicted and observed friction velocities are shown in Fig. 4b, where an over-prediction is evident. Note that the vertical momentum fluxes, $\overline{u'w'}$ and $\overline{v'w'}$ are not computed in our MM5 computations. Instead, u_* is used to compute the convective velocity scale using vertical profile functions that invoke Monin-Obukhov length scale (i.e. $w_s = u_* \Phi_m^{-1}$) as well as for calculating vertical eddy diffusivities. In so doing, the MRF scheme in the control run employs a cut-off (minimum) value of $u_* = 0.1 \text{ m s}^{-1}$. Imposing such constraints is common to ensure computational stability of numerical codes, and in the control and modified runs this minimum value was left unaltered. Such an imposed minimum, however, has plagued the comparison of measurements and predictions of Fig. 4, where most of the nocturnal and a part of the convective periods are dominated by very low u_* ($< 0.1 \text{ m s}^{-1}$). We performed sensitivity studies with different cut-off value of u_* , which will be discussed later. All three schemes, therefore, showed

almost identical and constant u_* during the night. Some deviations (or bumps) can be seen in nocturnal u_* (e.g. October 15th in Fig. 4b) due to a temporary increase of surface winds during that time (Fig. 4c). As expected, due to the use of the same parameterization scheme, the daytime u_* values are almost identical, but a significant over-prediction is evident. Such over-prediction of u_* is partly responsible for the over-prediction of the heat flux, given that u_* is used to compute the sensible heat flux.

4.3. Statistical Performance Measures

To further evaluate the models' performance, several standard statistical measures -- mean, standard deviation, root mean square error (RMSE) and mean difference -- were employed; the relevant formulae and methodologies can be found in Pielke and Pearce (1994) and Sivacoumar and Thanasekaran (2001). The mean indicates the central value about which the measurements are distributed, and for a good model the mean of measurements and predictions should be as close as possible. The standard deviation indicates how closely the variable is dispersed about the mean. The mean difference is the mean of the difference between the prediction and measurement, and RMSE is a measure of the error between the predictions and data (which is zero for an ideal model).

Considering the importance of surface properties in assessing human comfort as well as the health of ecosystems, it was decided to focus on the near surface wind speed, wind direction and temperature. Hourly averaged values collected from the 41 stations shown in Fig. 2 were used for the statistical evaluation. Winds weaker than 0.5 m s^{-1} were excluded, given inherent errors associated with measurements at low speeds. The

computation of statistical parameters is straightforward for the wind speeds and temperature, but due to the circular nature of the data wind-direction statistics pose a problem. As a remedy, the ‘modified wind direction’ was used, wherein 360^0 was either added to or subtracted from the predicted value to minimize the absolute difference between the observed and predicted wind directions. For example, if the prediction is 30^0 and the corresponding observation was 350^0 , then a predicted value of 390^0 was used (Lee and Fernando, 2004).

Since new parameterizations were implemented only for the stable period, statistics were computed separately for the daytime convective and nighttime stable periods. Based on sunset and sunrise times, the daytime was considered from 0700 MST to 1800 MST and the rest was considered nighttime. Sunset and sunrise times on October 7, 2000 in Salt Lake City were, respectively, 0631 MST and 1759 MST, and the corresponding values for October 16 were 0640 MST and 1745 MST. The calculated evaluation measures for the nocturnal and daytime periods are listed in Tables 1 and 2.

For the nocturnal period, as discussed in the previous section, MRF over-predicted the temperature (approximately 1 K) and wind speed (about 0.2 to 0.3 m s^{-1}), and the modified schemes generally reduced these deviations. Modified schemes also reduced the RMSEs for the prediction of all three variables. With respect to the wind direction, Modification 2 appears to perform marginally better compared to the other two. As expected, all three schemes showed comparable performance for the convective period.

Recall that the Day 16 case was dominated by local differential thermal forcing (i.e. thermal circulation) whereas the Day 7 case was signified by both synoptic and local forcing. Nevertheless, the general behavior of MRF for both days was similar, in that the

nocturnal temperature and wind speed were over-predicted and the daytime temperature and wind speed were under-predicted. Kindred qualitative behaviors were also noted for both days for other variables, such as radiation, heat flux, inversion strength, surface stress, etc (for brevity, the details are not repeated here). The modified schemes generally showed a better or comparable agreement with observations than the MRF scheme.

As for the difference between the predictions for two cases, the mean differences of daytime temperature are larger in the Day 16 case than in the Day 7 case (see Tables 1 and 2), suggesting that the modeled daytime temperature of the latter is higher. This is consistent with the manner MM5 accounts for the summer and winter seasons, that is the surface albedo changes on the October 15. Thus the Day 7 case, due to the smaller summer albedo, receives more solar irradiance than the Day 16 case.

In all, according to Tables 1 and 2, the modified runs outperformed the Control runs. We note, however, that the standard deviations and RMSEs for the daytime are generally larger for the modified schemes than for the MRF. The differences between the daytime simulations, despite the usage of the same parameterizations, arise due to the differences in the nighttime behavior, which carry over to the day through dynamical fields such as pressure and temperature gradients.

5. Further Sensitivity Runs on Pr , Rib_{cr} , and u^* dependence

There is a fundamental difference in the way that the modified and the control (MRF) schemes implement vertical heat diffusivity in MM5. As discussed in Section 2.1, the MRF scheme uses a constant Prandtl number (K_m / K_h) within the whole boundary layer regardless of stability, and for the stable case a Prandtl number of 1.3 ($K_h = 0.77 K_m$) is

used. Another popular default scheme of MM5, the Blackadar scheme (Blackadar, 1979; Zhang and Anthes, 1982), assumes a Prandtl number of unity, wherein K_h is set equal to K_m upon computing the latter as a function of the Richardson number and vertical wind shear.

In order to investigate whether the improved temperature predictions of modified runs is a result of the use of a more realistic Prandtl number (or stability dependent K_h and K_m), a sensitivity run was conducted with the same momentum diffusivity as modification 1 (eq. 10), but with a Prandtl number of unity. The results are shown in Figs. 7 and 8, together with observations; for robustness, time series of measurements averaged over 41 measurement stations of Fig. 2 are employed for comparisons. The modified runs clearly show better temperature performance than the sensitivity runs (Fig. 7a), although no striking differences could be found between the two for wind predictions. We also conducted a statistical analysis to evaluate the performance of the control run, two modifications and the sensitivity run using data from all 41 stations, and found that the modified runs give the best agreement with the data as far as the mean values are concerned.

When the unit Prandtl number is applied to modification 1, the vertical exchanges become similar to Blackadar or MRF schemes, and the heat is vertically exchanged with an equal or comparable diffusivity as momentum. This leads to a larger nocturnal downward heat flux and undue warming of the surface, giving rise to higher surface temperature. This warming is absent in the modified runs because of the lower heat diffusivities they permit at larger Richardson numbers.

Even though the same momentum diffusivity was used for the sensitivity run and Modification 1, the near surface wind fields for the two cases have noticeable differences. This can be ascribed to the mutual dependence of pressure gradient forces (that drives the wind) and temperature structure (determined by the heat diffusivity). For the Day 16 case, the nocturnal wind speed of the sensitivity run (Fig. 7b) is a bit weaker than that from Modification 1, perhaps due to the reduced temperature gradients as a result of enhanced vertical exchange. Predicted wind directions from the two schemes are in excellent agreement with measurements, showing the prominence of diurnal forcing (Fig. 7c). As shown in Fig. 8, for the Day 7 case, the nocturnal trends of temperature was similar to the Day 16 case, but the wind speeds tended to be slightly higher in the sensitivity run.

We performed several other tests by changing parameters that possibly influence near surface predictions. First, given that a small frictional velocity would decrease turbulent mixing in the boundary layer, thereby possibly lowering near-surface temperature closer to observations, a small cut-off value of $u_* = 0.01 \text{ m s}^{-1}$ was tested instead of the default value, 0.1 m s^{-1} . The configuration of the sensitivity run was identical to that of the control except the u_* value. The two runs produced almost identical results, indicating, as expected, local shear instabilities in the stratified layer control the mixing rather than the wall shear production. When averaged over the 41 stations shown in the Fig. 2, minimum temperature at 0600 MST Oct 16th simulated by the sensitivity test was 279.32 K, while the corresponding values from the control and the measurements were 279.08 K and 277.72 K, respectively.

In the second test, the boundary layer depth for stable condition was modified by changing critical bulk Richardson number, Rib_{cr} in eq (8). The boundary layer is defined as the region where the bulk PBL Richardson number exceeds a critical value, and thus a low Rib_{cr} was expected to result in a reduced PBL depth and consequently reduced PBL mixing. A test run was performed with $Rib_{cr} = 0.25$ instead of 0.5, a default value, in which other than the Rib_{cr} , all the settings and parameters were identical to those of the control. Again, simulation results from the test run were almost same as those from the control. The 41 station-averaged minimum temperatures at 0600 MST Oct 16th from the sensitivity test was 279.27 K, while the corresponding value from the control was 279.08 K. Therefore, we concluded that the improvements of predictions of the modified schemes was attributed to the realistic treatment of heat and momentum diffusivities and their Ri_g dependence under large Ri_g conditions.

6. Summary and Conclusions

Two new turbulence parameterizations for stable (nocturnal) atmosphere based on the VTMX field campaign proposed by Monti et al. (2002) were implemented in MM5. In the first, dimensional forms of eddy diffusivities, expressed as a function of gradient Richardson number (Modification 1), were used whereas Modification 2 employed diffusivities normalized by the variance of vertical velocity and vertical wind shear. A unique contribution of this parameterization is the implementation of a stability varying turbulent Prandtl number that allows momentum to be carried away from a region by the internal wave, while heat diffusion by turbulent eddies being suppressed by the stable stratification. It was argued that the default PBL schemes of MM5 such as MRF or

Blackadar scheme tend to systematically over-predict turbulent diffusion of heat under stable conditions when a stability-independent turbulent Prandtl number is employed.

Simulations based on these modifications were conducted for the Salt Lake City airshed to simulate four IOPs that represented two different synoptic conditions. The Day 16 case was dominated by local differential thermal forcing, where well defined slope flows and a land-water contrast were evident, and the Day 7 case was signified by large-scale meteorological effects as well as local forcing. The modified schemes showed an improvement in predicting the nocturnal near surface temperature, in that it represented the stability dependence of vertical exchange coefficients better than the control case that utilized the MRF scheme. As a result, the surface sensible heat flux became smaller and the near surface inversion strength was intensified in comparison to that of the control runs, which turns out to be a better fit for observations. Only a slight improvement in wind speed predictions could be seen by the modified schemes, however, perhaps owing to the fact that the sensitivity of mean winds to the vertical exchange of momentum is not as straightforward as its temperature counterpart; in the former, for example, pressure gradient forces determined by the thermal structure, in addition to vertical momentum exchange, is a key factor. Statistical measures such as mean, standard deviation, RMSE and mean difference indicate that the modified schemes outperformed MRF.

A sensitivity run was conducted to study the influence of turbulent Prandtl number (the ratio of turbulent momentum diffusivity to heat diffusivity) on model predictions, considering that some default PBL schemes, including MRF, consider it as a constant. Recent measurements (Monti et al., 2002; Strang and Fernando, 2001) show that momentum is transferred more effectively than heat under stably stratified conditions,

possibly due to effective momentum (not heat) transport by internal waves. When the heat diffusivity was assigned a value that is the same or a significant fraction of the momentum diffusivity, the nocturnal near surface temperature increased by a few degrees compared to Modification 1. This owes to the artificial enhancement of vertical exchange between warmer upper and colder near-surface air masses.

References:

- Ballard, S. P., Golding, B. W., and Smith, R. N. B.: 1991, 'Mesoscale model experimental forecasts of the Haar of northeast Scotland', *Mon. Wea. Rev.*, **119**, 2107-2123.
- Benoit, R., Cote, J., and Mailhot, J.: 1989, 'Inclusion of a TKE boundary layer parameterization in the Canadian regional finite-element model', *Mon. Wea. Rev.*, **117**, 1726-1750.
- Berkowicz, R., and Prahm, L. P.: 1979, 'Generalization of K-theory for turbulent diffusion. Part I. Spectral diffusivity concept', *J. Appl. Meteorol.*, **18**, 266-272.
- Berkowicz, R., and Prahm, L. P.: 1980, 'On the spectral turbulent diffusivity theory for homogeneous turbulence', *J. Fluid Mech.*, **100**, 433-448.
- Blackadar, A. K.: 1979, 'High resolution models of the planetary boundary layer', in J. Pfafflin and E. Ziegler (eds.), *Advances in Environmental Science and Engineering*, Vol. 1, Gordon and Breach, pp. 50-85.
- Blumen W., (ed) 1990: Atmospheric processes over complex terrain, *Meteorol. Monogr.*, Vol 23, No. 45, Amer. Meteorol. Soc., 323pp

- Bright, D. R., and Mullen, S. J.: 2002, 'The sensitivity of the numerical simulation of the Southwest monsoon boundary layer to the choice of PBL turbulence parameterization in MM5', *Wea. Forecasting*, **17**, 99-114.
- Brown, A. R., Derbyshire, S. H., and Mason, P. J.: 1994, 'Large Eddy Simulation of stable atmospheric boundary layers with a revised stochastic subgrid model', *Quart. J. Roy. Meteorol. Soc.*, **120**, 1485-1512.
- Chen, F., and Dudhia, J.: 2001, 'Coupling an advanced land-surface/hydrology model with the Penn State/NCAR MM5 modeling system. Part I: Model implementation and sensitivity', *Mon. Wea. Rev.*, **129**, 569-585.
- Corrsin, S.: 1974, 'Limitations of gradient transport models in random walks and in turbulence', *Adv. Geophys.*, **18A**, 25-60.
- Derbyshire, S. H.: 1999, 'Stable boundary-layer modeling: Established approaches and beyond', *Boundary-Layer Meteorol.*, **90**, 423-446.
- Doran, J. C., Fast, J. D., and Horel, J.: 2002, 'The VTMX 2000 campaign', *Bull. Amer. Meteorol. Soc.* **83**, 537-551.
- Estoque, M. A.: 1968, 'Vertical mixing due to penetrative convection', *J. Atmos. Sci.*, **25**, 1046-1051.
- Fernando, H. J. S.: 2002, 'Turbulence in stratified flows', in R. Grimshaw (ed.), *Environmental Stratified Flows*, Kluwer Publishing, pp. 163-192.
- Fernando, H. J. S.: 2003, 'Turbulence patches in a stratified shear flow', *Phys. Fluids*, **15(10)**, 3164-3169.
- Fiedler, B. H.: 1984, 'An integral closure model for the vertical turbulent flux of a scalar in a mixed layer'. *J. Atmos. Sci.*, **41**, 674-680.

- Gargett, A.E. and Holloway, G.: 1992, 'Sensitivity of the GFDL Ocean Model to Different Diffusivities for Heat and Salt', *J. Phys. Oceanogr.*, **22**, 1158-1177.
- Holtslag, A. A. M., and Moeng, C.-H.: 1991, 'Eddy diffusivity and countergradient transport in the convective atmospheric boundary layer', *J. Atmos. Sci.*, **48**, 1690-1698.
- Hong, S.-Y., and Pan, H.-L.: 1996, 'Nonlocal boundary layer vertical diffusion in a medium-range forecast model', *Mon. Wea. Rev.*, **124**, 2322-2339.
- Janjic, Z. I.: 1990, 'The step-mountain coordinate: Physical package', *Mon Wea. Rev.*, **118**, 1429-1443.
- Janjic, Z. I.: 1994, 'The step-mountain eta coordinate model: Further developments of the convection, viscous sublayer, and turbulence closure schemes', *Mon. Wea. Rev.*, **122**, 927-945.
- Lee, S. M. and Fernando, H. J. S.: 2004, 'Evaluation of Mesoscale Meteorological Models, MM5 and HOTMAC using PAFEX-I data', *J. Appl. Meteorol.* **43**, 1133-1148.
- Louis, J. F.: 1979, 'A parametric model of vertical eddy fluxes in the atmosphere', *Boundary-Layer Meteorol.* **54**, 187-202.
- Mahrt, L, Sun, J., Blumen, W., Delany, T., and Oncley, S.: 1999, 'Nocturnal boundary-layer regimes', *Boundary-Layer Meteorol.* **88**, 255-278.
- McNider, R. T., England, D. E., Friedman, M. J., and Shi, X.: 1995, 'Predictability of the stable atmospheric boundary layer', *J. Atmos. Sci.*, **52**, 1602-1614.
- Mellor, G. L. and Yamada, T.: 1974, 'A hierarchy of turbulence closure models for planetary boundary layers', *J. Atmos. Sci.*, **31**, 1791-1806.

- Monti, P, Fernando, H. J. S., Princevac, M., Chan, W. C., Kowalewski, T. A., Pardyjak, E. R.: 2002, 'Observations of flow and turbulence in the nocturnal boundary layer over a slope', *J. Atmos. Sci.*, **59**, 2513-2534.
- Nieuwstadt F. T. M.: 1984, 'The turbulent structure of the stable, nocturnal boundary layer', *J. Atmos. Sci.* **41**, 2202-2216.
- Pan, Z., Benjamin, S., Brown, J. M., and Smirnova, T.: 1994, 'Comparative experiments with MAPS on different parameterization schemes for surface moisture flux and boundary layer processes', *Mon. Wea. Rev.*, **122**, 449-470.
- Pacanowski, R.C., and Philander, S.G.H.: 1981, 'Parameterization of vertical mixing in numerical models of the tropical oceans'. *J. Phys. Oceanogr.* **11**, 1443-1451.
- Pielke, R. A., and Pearce, R. P.: 1994, *Mesoscale modeling of the atmosphere*, Meteorol. Monogr., Vol 25, No. 47, Amer. Meteorol. Soc., 156pp.
- Poulos, G.S., Blumen, W., Fritts, D. C., Lundquist, J., Sun, J., Burns, S. P., Nappo, C., Banta, R., Newsom, R., Cuxart, J., Terradellas, E., Balsley, B., and Jensen, M.: 2002, 'CASES-99: A comprehensive investigation of the stable nocturnal boundary layer', *Bull. Amer. Meteorol. Soc.*, **83**, 521-536.
- Riley, J. J., and Lelong, M. P.: 2000, 'Fluid motions in the presence of strong stable stratification', *Ann. Rev. Fluid Mech.*, **32**, 613-657.
- Rotach, M. W. and others: 2004, 'Turbulence structure and exchange processes in an Alpine valley: the Riviera Project', *Bull. Amer. Meteorol. Soc.*, **85**, 1367-1385.
- Sivacoumar, R., and Thanasekaran, K.: 2001, 'Comparison and performance evaluation of models used for vehicular pollution prediction', *J. Environ. Eng.*, **127**, 524-530.

- Strang, E. J., and Fernando, H. J. S.: 2001, 'Vertical mixing and transports through a stratified shear layer'. *J. Phys. Oceanogr.*, **31**, 2026-2048.
- Stull, R. B.: 1988', *An introduction to boundary layer meteorology*. Kluwer Academic Publishers, 666pp.
- Stull, R. B.: 1993, 'Review of non-local mixing in turbulent atmospheres: Transilient turbulence theory', *Bound.-Layer Meteorol.*, **62**, 21-96.
- Townsend, A. A.: 1980, *The structure of turbulent shear flow*. Cambridge Univ. Press, Cambridge', U.K., 440 pp.
- Troen, I., and Mahrt, L.: 1986, 'A simple model of the atmospheric boundary layer: Sensitivity to surface evaporation', *Bound.-Layer Meteorol.*, **37**, 129-148.
- Whiteman, C. D.: 2000, *Mountain meteorology: fundamentals and applications*. Oxford University Press. 355 pp.
- Wyngaard, J. C., and Brost, R. A.: 1984, 'Top-down and bottom-up diffusion of a scalar in the convective boundary layer', *J. Atmos. Sci.*, **41**, 102-112.
- Xiu, A., and Pleim, J. E.: 2000, 'Development of a land surface model. Part I: Application in a mesoscale meteorology model'. *J. Appl. Meteorol.*, **40**, 192-209.
- Yamada, T.: 1983, 'Simulations of nocturnal drainage flows by a q2l turbulence closer model', *J. Atmos. Sci.*, **40**, 91-106.
- Yamada, T., and Bunker, S.: 1988, 'Development of a nested grid, second moment turbulence closure model and application to the 1982 ASCOT Brush Creek data simulation', *J. Appl. Meteorol.*, **27**, 562-578.

- Zhang, D., and Anthes, R. A.: 1982, 'A high-resolution model of the planetary boundary layer – sensitivity tests and comparisons with SESAME-79 data', *J. Appl. Meteorol.*, **21**, 1594-1609.
- Zhang, D-L., and Zheng, W-Z.: 2004, 'Diurnal cycle of surface winds and temperature as simulated by five boundary layer parameterizations', *J. Appl. Meteorol.*, **43**, 157-169.
- Zhong, S., and Fast, J.: 2003, 'An evaluation of MM5, RAMS, and Meso Eta at sub-kilometer resolution using VTMX field campaign data in the Salt Lake Valley', *Mon. Wea. Rev.* **131**, 1301-1322.

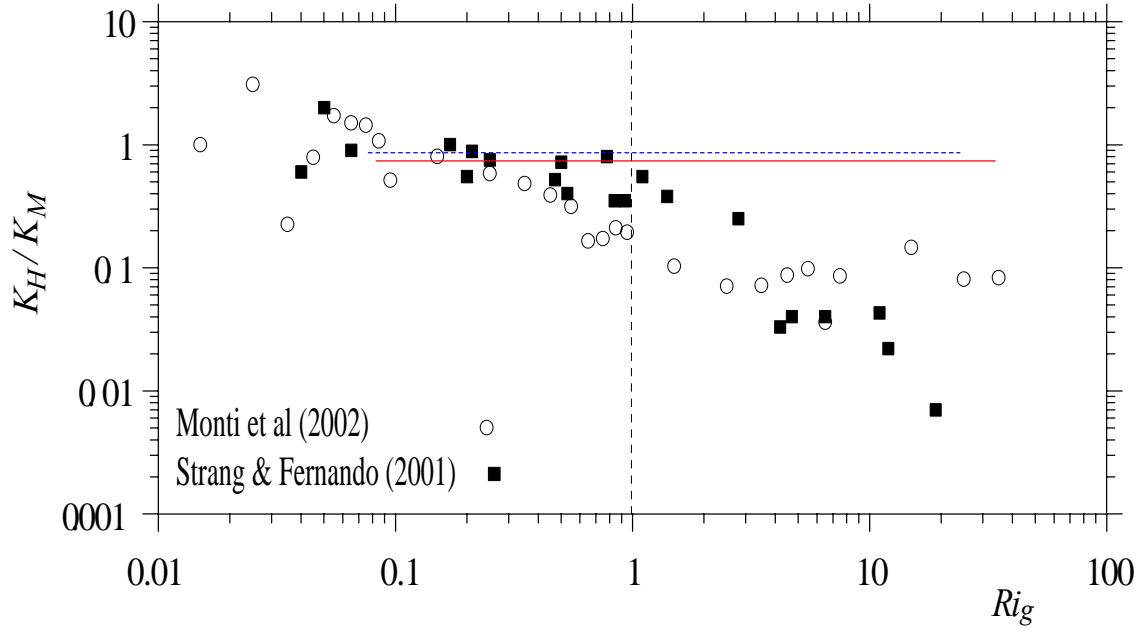


Fig. 1. The ratio of heat to momentum eddy diffusivity as a function of the gradient Richardson number. Open circles and filled squares are from field measurements of Monti et al (2002) and laboratory data of Strang and Fernando (2001), respectively. The ratio of eddy diffusivities employed in the MRF and the Blackadar PBL scheme are represented by a solid line and a dotted line, respectively.

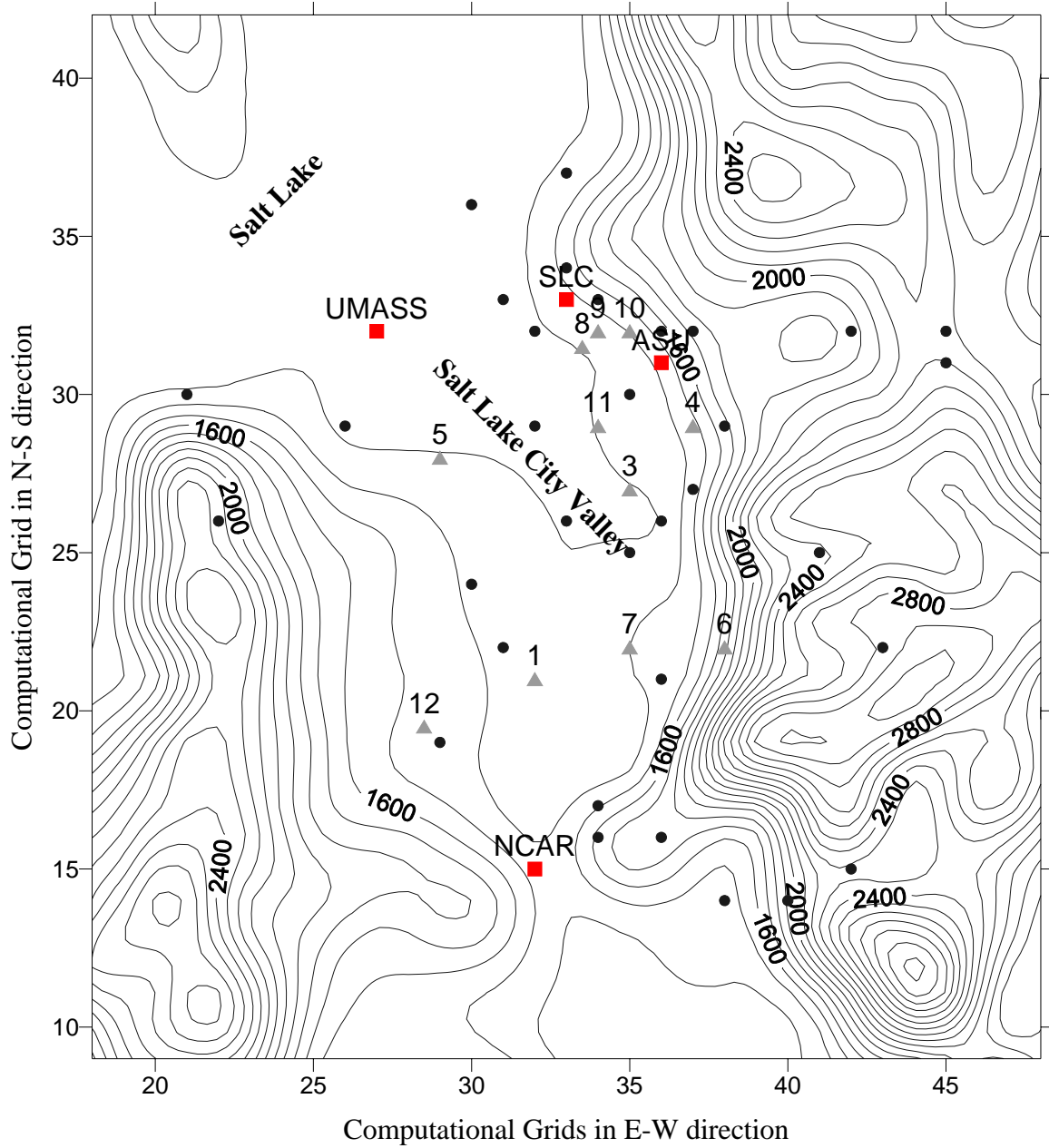


Fig. 2. The topography and the locations of measurements sites in the Salt Lake City basin. Sites specifically discussed in the paper are marked by filled squares, the sites referred to as VPN Sites are marked by filled triangles. The numbers adjacent to these triangles indicate the VPN Site number (e.g. VPN09). ASU represents the Arizona State University site operated by our group. For further details, see Doran et al. (2002).

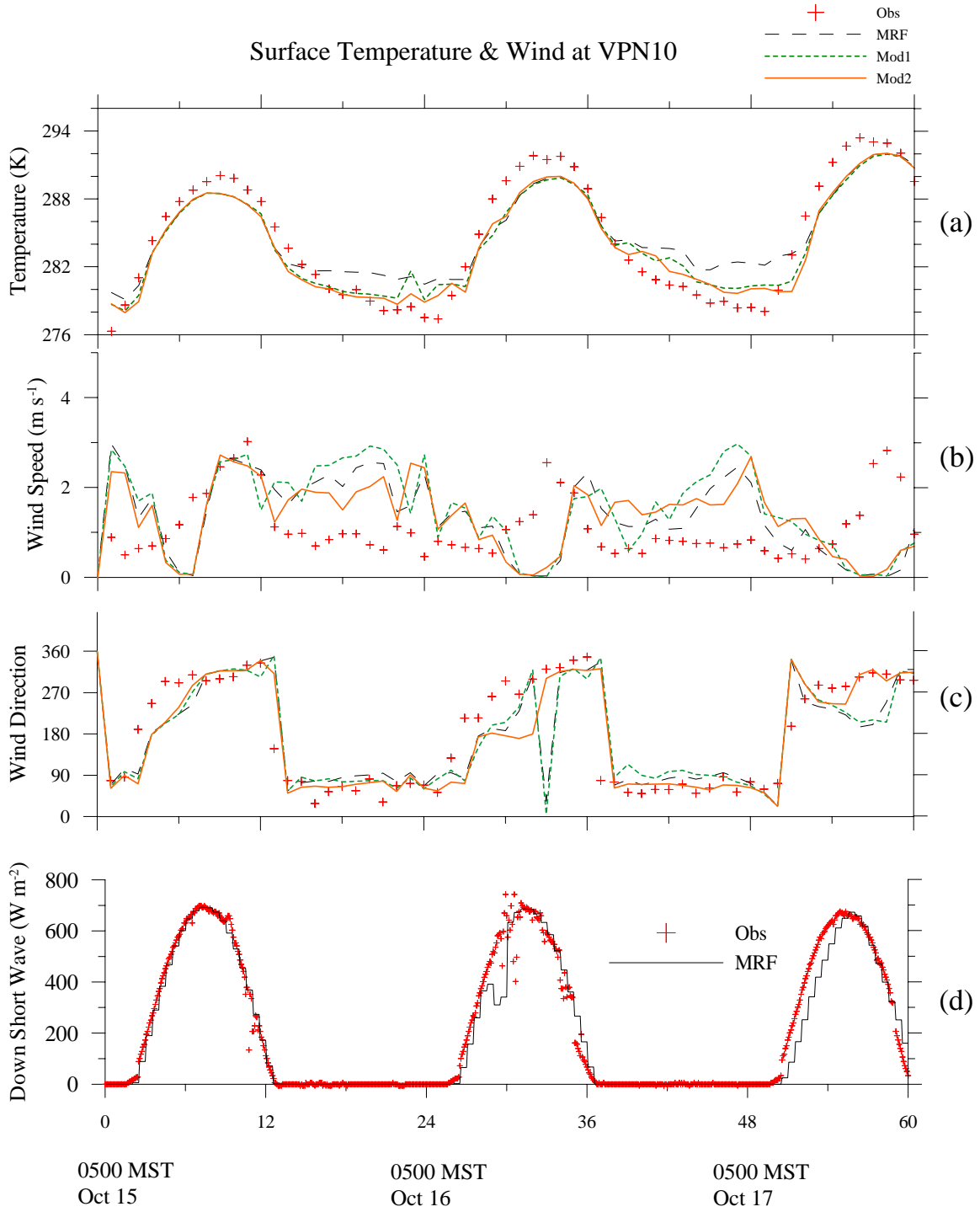


Fig. 3. Times series of predicted and observed near surface temperature, wind speed and wind direction for the Day 16 case. The observations were taken at a single station VPN10, every 5 minutes. Observed and predicted downward shortwave radiation from MRF at the ASU site are presented as well.

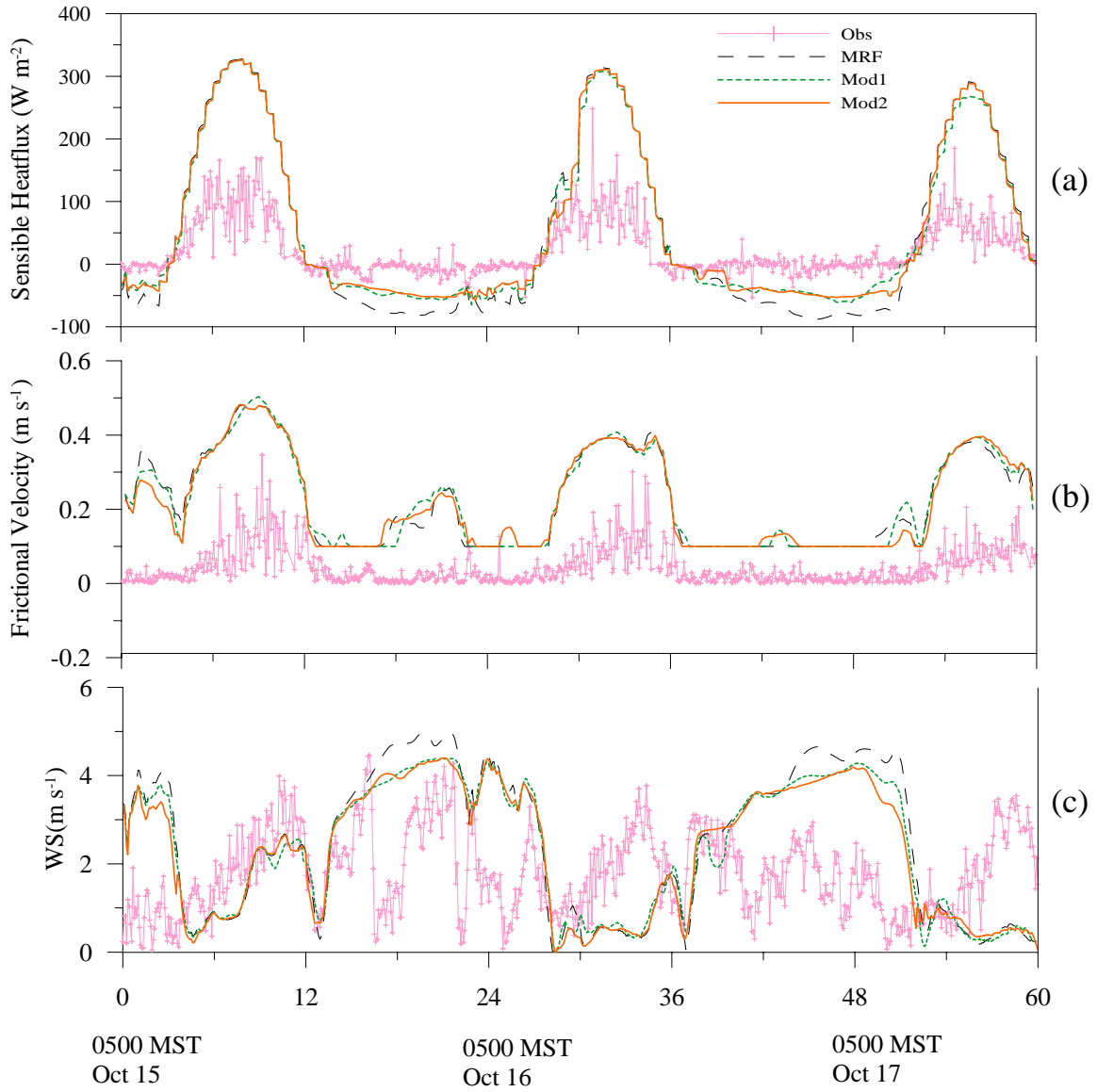


Fig. 4. Times series of predicted and observed surface sensible heat flux, the surface frictional velocity and wind speed at the ASU site for the Day 16 case. The observations are averaged over 5 minutes from 10 Hz sonic data.

Jordan Narrow

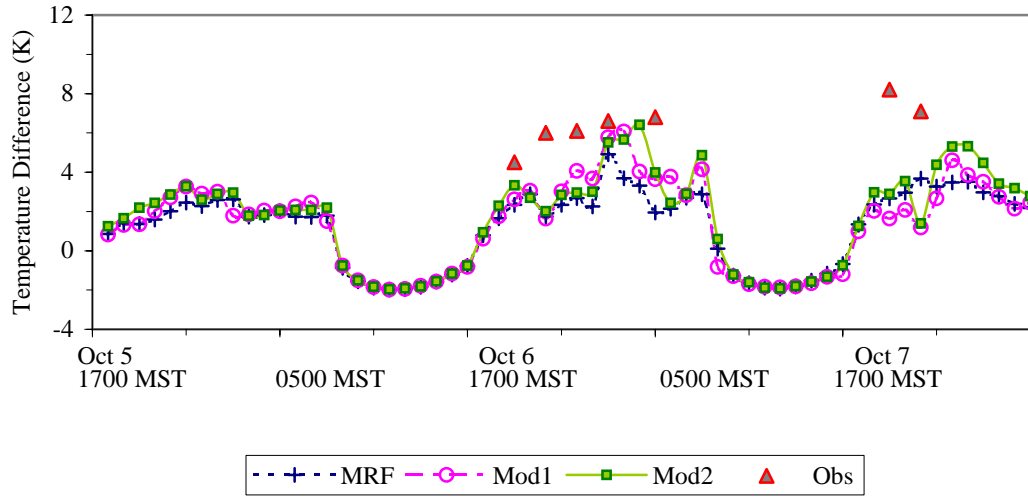


Fig. 5. Time series of predicted and observed temperature difference, ΔT , between 2 m and approximately 55 m agl at the NCAR site for the Day 16 case. Available rawinsonde data during the simulation period are presented.

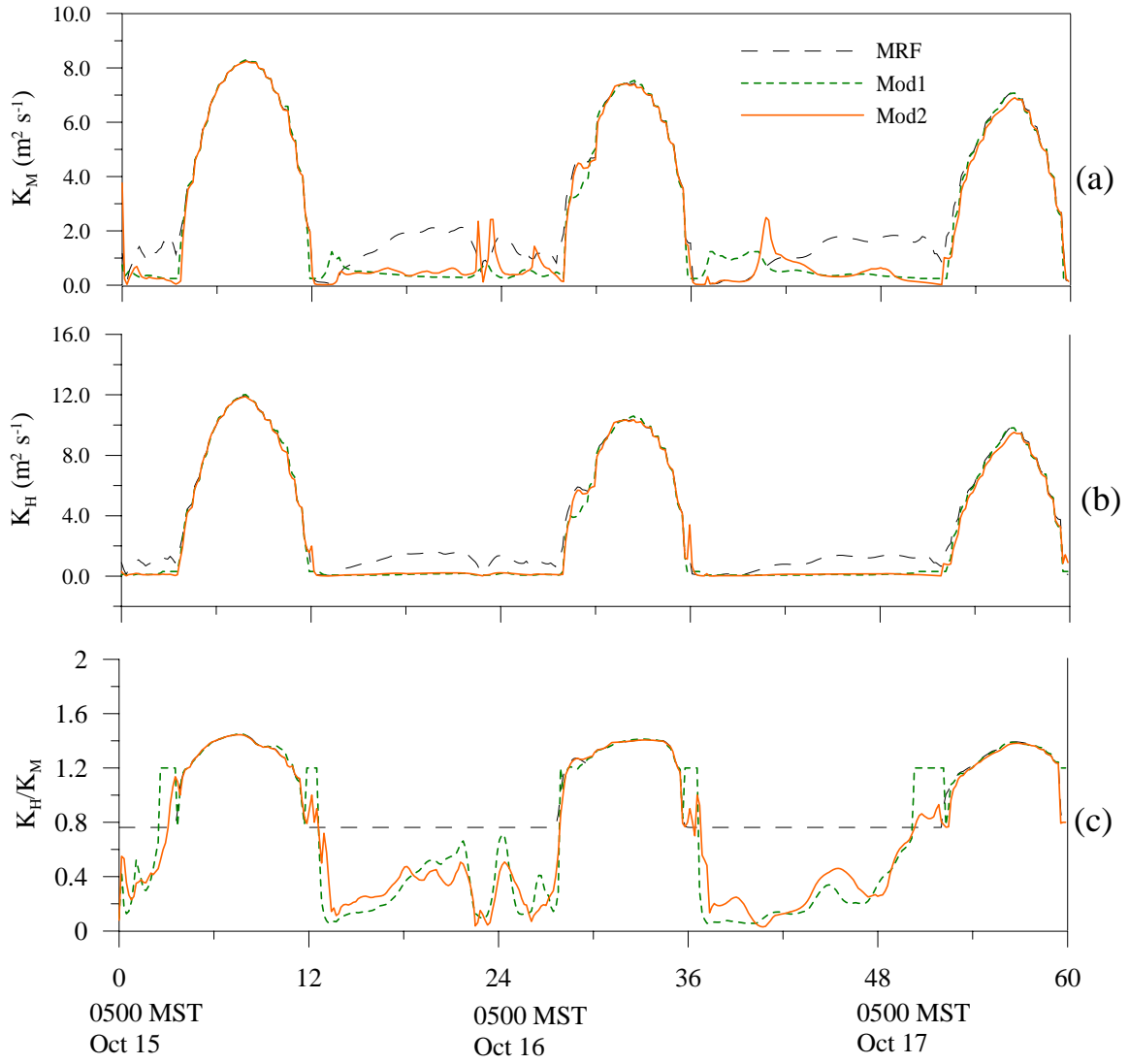


Fig. 6. The simulated vertical diffusion coefficients for (a) momentum, (b) heat and (c) the ratio of the two (inverse Prandtl number) at the ASU site for the Day 16 case.

Averaged Surface Temperature & Wind For Day 16th Case

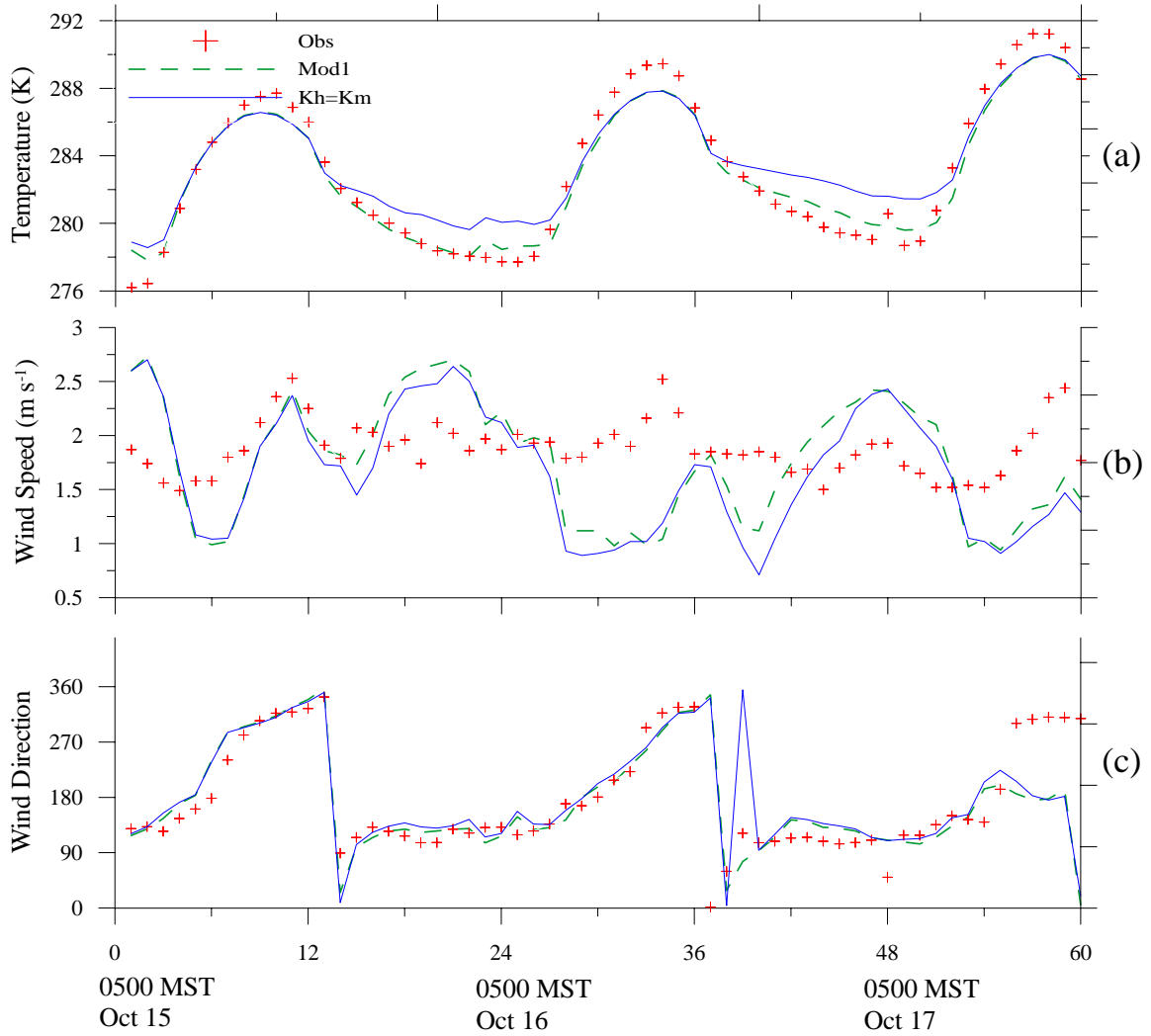


Fig. 7. Time series of simulated and observed near surface temperature, wind speed and wind direction for the Day 16 case. The observations are hourly average among available measurements from all 41 stations marked in Fig. 1.

Averaged Surface Temperature & Wind For Day 7th Case

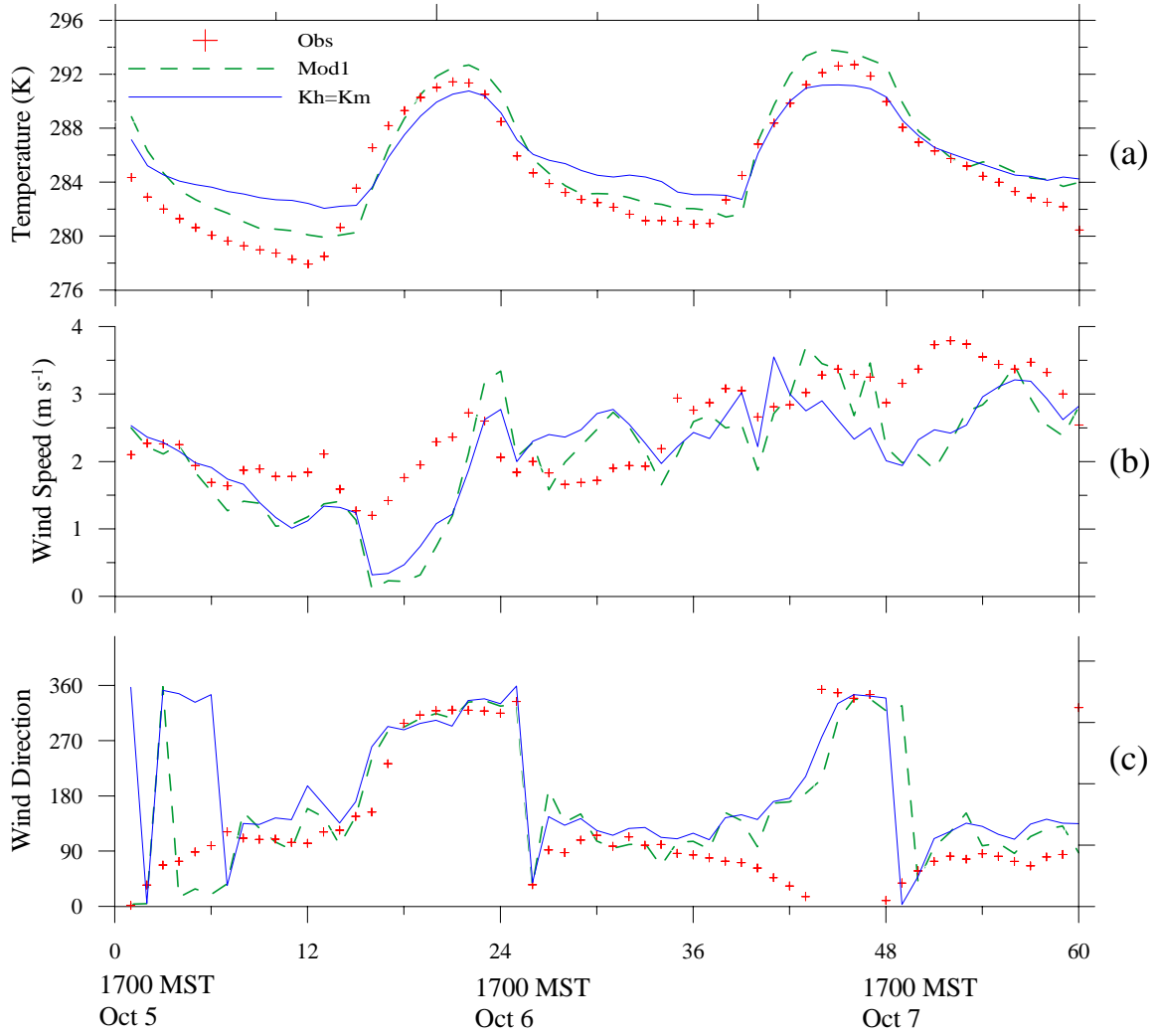


Fig. 8. Same as Fig. 7 except the Day 7 case.

Tables

Table 1. Model mean, standard deviation, RMSE, and mean difference for surface temperature, wind speed and wind direction based on hourly values of 41 stations in the vicinity of the Salt Lake Valley for the Day 16 case.

Category	Variables	Statistics	Obs	MRF	Mod1	Mod2
Night	Temperature (K)	Mean	279.71	280.64	280.13	280.10
		STD	3.05	2.33	2.47	2.51
		RMSE		2.38	2.34	2.36
		MeanDiff		-0.96	-0.45	-0.41
	Wind Speed (m/s)	Mean	1.85	2.07	2.13	1.95
		STD	1.25	1.24	1.15	1.14
		RMSE		1.63	1.56	1.58
		MeanDiff		-0.23	-0.29	-0.11
	Wind Direction (degree)	Mean	135.86	140.02	142.91	137.84
		STD	76.20	90.34	92.47	90.24
		RMSE		75.72	75.93	74.58
		MeanDiff		-4.07	-7.07	-1.83
Day	Temperature (K)	Mean	285.50	284.77	284.64	284.69
		STD	4.86	4.19	4.31	4.40
		RMSE		2.89	2.91	2.90
		MeanDiff		0.73	0.86	0.81
	Wind Speed	Mean	1.91	1.55	1.54	1.43

	(m/s)	STD	1.20	1.18	1.11	1.08
		RMSE		1.52	1.49	1.51
		MeanDiff		0.35	0.37	0.48
Wind Direction (degree)		Mean	211.99	209.64	209.02	210.89
		STD	102.07	120.50	121.59	124.22
		RMSE		81.06	80.79	81.79
		MeanDiff		2.35	2.97	1.10

Table 2. Same as Table 1 except the Day 7 case.

Category	Variables	Statistics	Obs	MRF	Mod1	Mod2
Night	Temperature (K)	Mean	282.10	283.01	282.49	281.80
		STD	3.58	2.58	2.62	2.72
		RMSE		2.98	3.10	3.26
		MeanDiff		-0.91	-0.39	0.30
	Wind Speed (m/s)	Mean	2.47	2.81	2.70	2.61
		STD	2.34	2.08	1.50	1.55
		RMSE		2.28	2.32	2.28
		MeanDiff		-0.34	-0.22	-0.13
	Wind Direction (degree)	Mean	138.30	135.59	141.33	135.48
		STD	86.16	114.98	112.77	115.83
		RMSE		82.33	80.24	81.05
		MeanDiff		2.54	-3.21	2.65
Day	Temperature (K)	Mean	288.66	288.05	288.20	288.22
		STD	4.06	3.86	4.03	4.12
		RMSE		2.84	2.97	3.00
		MeanDiff		0.61	0.46	0.44
	Wind Speed (m/s)	Mean	2.50	2.17	2.34	2.05
		STD	1.91	1.64	1.62	1.53
		RMSE		1.89	2.28	2.22

		MeanDiff		0.33	0.16	0.45
	Wind	Mean	205.47	203.25	210.58	207.45
	Direction	STD	119.77	149.37	146.77	147.43
	(degree)	RMSE		75.63	88.62	86.13
		MeanDiff		2.22	-5.11	-1.98